



## Effects of ozone addition on the kinetics and efficiencies of methane conversion at fuel-rich conditions

Wenwen Xie<sup>\*</sup>, Simon Drost, Robert Schießl, Ulrich Maas

*Institute of Technical Thermodynamics, Karlsruhe Institute of Technology, Karlsruhe, 76131, Germany*

### ARTICLE INFO

#### Keywords:

Ozone addition  
Chemical kinetics  
Polygeneration processes  
Chemical energy storage  
Rapid compression machine

### ABSTRACT

Compression–expansion processes have the potential of converting mechanical work to chemical energy at fuel-rich conditions, allowing for the storage of fluctuating renewable energies. In this work, the conversion of methane and natural gas (NG) is investigated for this purpose. A focus is on using ozone as a reaction promoter for the otherwise slow reaction. The kinetics of fuel-rich methane/NG oxidation with ozone addition is investigated experimentally and numerically. To this end, ignition delay times (IDTs) for CH<sub>4</sub>/O<sub>2</sub>/O<sub>3</sub>/Ar and NG/O<sub>2</sub>/O<sub>3</sub>/Ar mixtures are measured in a rapid compression machine (RCM). It is shown that a reaction mechanism obtained by simply combining a previously developed mechanism for methane conversion (PolyMech2.0) with an ozone sub-mechanism does not accurately predict IDTs. Sensitivity analyses identify reactions in the methane submechanism that become more important for ignition delay time when ozone is added in comparison to mixtures without O<sub>3</sub>. The rate coefficients of these reactions are modified within their uncertainty ranges to better match the experimentally obtained IDTs. The resulting kinetic model, named PolyMech 3.0, predicts the IDTs obtained in RCM-experiments well. Analysis reveals a two-fold promoting effect of ozone addition on methane/air ignition: Ozone causes a temperature rise by the reactions associated with its decomposition. Ozone also forms reactive products such as hydrogen and oxygen radicals, which can then promote reactions of the hydrocarbons. Quantitative analysis shows that the latter effect is more pronounced. Using PolyMech 3.0, parametric simulation studies for methane conversion in four-stroke engine cycles are carried out to explore the effects of ozone addition on chemical energy storage and efficiencies of engine-based polygeneration processes. Results show that with ozone addition, methane conversion can take place at high engine speeds, while without ozone, there is nearly zero conversion of fuel rich methane mixtures because of the low reactivity. Therefore, ozone addition allows for reasonable efficiencies across a wider range of operating conditions.

### 1. Introduction

The utilization of renewable energies to replace fossil fuels is substantial for achieving a climate-neutral economy. However, renewable energies such as solar and wind power have massive fluctuations, and their availability is not always consistent with the power demand [1]. As a result, energy storage is becoming increasingly important as a means to level out local and temporal discrepancies between energy demand and supply.

Chemical energy carriers combine advantages of high energy capacity and long discharge duration. Polygeneration processes, which can convert mechanical power to chemical energy and, on demand, produce heat and work, are a way for achieving chemical energy storage [2,3]. The mechanical power required for the conversion is assumed to be derived from a surplus of renewable energies. Polygeneration process can operate at fuel-rich conditions to produce useful chemicals such as

H<sub>2</sub> and CO [4–6], or larger hydrocarbons like C<sub>2</sub>H<sub>2</sub> and C<sub>2</sub>H<sub>4</sub> [7–9] from methane or natural gas (NG). Therefore, these processes are different from combustion-based power generation processes, which aims at complete oxidation of fuels under fuel-lean or near-stoichiometric conditions. The reactants considered here, methane or natural gas, have low carbon content. Since the transition from fossil fuels to carbon-free fuel such as hydrogen will take time, methane could be a viable short-to-medium-term solution due to its high abundance [10]. Besides, methane, one of the most abundant greenhouse gas, is emitted by human-related activities and could be captured for usage [11].

Kinetic models for the underlying chemical reactions are necessary for the prediction and optimization of polygeneration processes. Over the past decades, chemical kinetic models describing methane oxidation in stoichiometric or fuel-lean conditions have become readily available. In contrast, reaction mechanisms targeting ultra-rich conditions

<sup>\*</sup> Corresponding author.

E-mail addresses: [wenwxie@qq.com](mailto:wenwxie@qq.com) (W. Xie), [robert.schiessl@kit.edu](mailto:robert.schiessl@kit.edu) (R. Schießl).

<https://doi.org/10.1016/j.jaecs.2023.100157>

Received 10 May 2022; Received in revised form 15 May 2023; Accepted 4 June 2023

Available online 8 July 2023

2666-352X/© 2023 Published by Elsevier Ltd. This is an open access article under the CC BY-NC-ND license (<http://creativecommons.org/licenses/by-nc-nd/4.0/>).

are less well-developed. Based on existing models and experimental data from an rapid compression machine (RCM), a flow-reactor, and a shock-tube at stoichiometric and fuel-rich conditions, a kinetic model, PolyMech 1.0, describing CH<sub>4</sub>/dimethyl ether (DME) polygeneration processes was developed [12]. To include accurate predictions of certain species profiles such as CO, H<sub>2</sub>, and C<sub>6</sub>H<sub>6</sub>, an improved mechanism, PolyMech 2.0, was then obtained by updating reaction rate constants based on the sensitivity analysis and including the reaction pathways for the formation of polycyclic aromatic hydrocarbons (PAH) [8].

Because of the low reactivity of methane, in aforementioned studies DME was added as a reaction enhancer at a concentration of 5–10 mol% in fuel [12]. It was later found that the fraction of fuel energy from the reaction enhancer, DME, was relatively high, roughly 10%–20% of the total energy in the fuel/reaction enhancer mixture, which is economically inefficient due to the high cost of DME production. Ozone was then demonstrated to be an effective reaction-enhancing additive in combination with DME [13]. Experimental results in a homogeneous-charge compression-ignition (HCCI) engine showed that ozone can significantly reduce the amount of DME required for the same reaction enhancing effect, namely from 11.0% required DME without O<sub>3</sub> to only 5.3% DME when combined with 75 ppm O<sub>3</sub>. But pure ozone addition has not been experimentally investigated in [13] due to the ozone generator's capacity limitation.

In this study, we investigate polygeneration processes of methane and a NG surrogate (90 mol% CH<sub>4</sub>, 9 mol% C<sub>2</sub>H<sub>6</sub> and 1 mol% C<sub>3</sub>H<sub>8</sub>) using ozone as the sole additive. Ignition delay times are measured in a RCM at a compression pressure of 20 bar, a compression temperature range of 950–1300 K and O<sub>3</sub> concentration of 310–910 ppm. A first kinetic model for CH<sub>4</sub>/NG/O<sub>3</sub> chemistry is obtained by combining PolyMech 2.0 with the ozone sub-mechanism in [14]. This combined model is referred to as PolyMech 2.01. PolyMech 2.01 predicts the IDTs well for mixtures without ozone well, but over-predicts the IDTs of mixtures with ozone addition. To improve the model, we use sensitivity and uncertainty analyses of reactions with respect to pressure and heat release rate evolution to determine rate coefficients for a set of sensitive reactions which are optimized within their uncertainties. This results in an updated kinetic model, PolyMech 3.0, which predicts RCM-IDTs reasonably well.

Another question is how the ozone addition affects the efficiencies of polygeneration processes, specifically the efficiencies of chemical energy storage and work output. To this end, parametric studies for four-stroke engines cycles are conducted using PolyMech 3.0, and the results are analyzed.

The remainder of this manuscript is organized as follows. The methodology of experiments and simulations is described in Section 2; the development of kinetic model is presented in Section 3. The following Section 4 describes parametric studies, based on the newly improved reaction mechanism, which assess the potential of the conversion for energy storage and chemical conversion under typical, technically readily accessible, piston-engine conditions. Conclusions are finally provided in Section 5.

## 2. Methodology

### 2.1. Experiment

Experiments are carried out in a RCM, which is a piston-cylinder device for studying chemical reactions in compressed, hot gases under well-controlled conditions.

The following procedure is applied for conducting an experiment: The RCM combustion chamber is first evacuated, then filled with the gas mixture to be investigated. This gas is then compressed by pneumatically pushing the piston to the top dead center (TDC). The short compression time (20–40 ms) renders the process nearly adiabatic, leading to high gas temperatures and pressures at the end of compression. The piston is mechanically locked when it reaches TDC, such that

**Table 1**

Technical data of the RCEM used in this work.

Bore $B$	82 mm
Stroke $S$	76–78 mm
Compression ratio $\epsilon$	6.8–17
Mixing vessel, Volume $V_M$	≈ 20 l
Compression time $\tau_c$	≈ 20–40 ms

**Table 2**

Mixture compositions investigated in RCM experiments. O<sub>3</sub> concentration in ppm, other compositions in mol%,  $\phi = 2.0$ .

Case name	%CH <sub>4</sub>	%C <sub>2</sub> H <sub>6</sub>	%C <sub>3</sub> H <sub>8</sub>	%O <sub>2</sub>	O <sub>3</sub> (ppm)	%Ar
CH <sub>4</sub>	5	–	–	5	–	90
NG	4.32	0.432	0.048	5.19	–	90
CH <sub>4</sub> + O <sub>3</sub>	5.02	–	–	4.89	910 (±80)	90
NG + O <sub>3</sub>	4.33	0.433	0.048	5.16	315 (±32)	90

isochoric conditions prevail afterwards. The compressed gas is allowed to react, and when auto-ignition occurs, exothermal reactions cause a pronounced pressure rise. By detecting time-resolved in-cylinder pressure traces, the time between the end of compression and the onset of the ignition-induced pressure rise can be determined experimentally. This time is defined as the ignition delay time (IDT).

IDTs in Arrhenius diagrams are commonly reported in dependence of the compression temperature  $T_C$ , determined from the experimentally measured pressure  $p_C$  via an isentropic/adiabatic core model. For O<sub>3</sub>-containing mixtures, reactions may occur before the end of compression due to the fast decomposition of O<sub>3</sub>. To assess the influence of pre-compression reactions on the assigned compression temperature, a series of simulations of auto-ignition events was conducted. In these simulations, a CH<sub>4</sub>/O<sub>2</sub>/O<sub>3</sub> mixture with  $\phi = 2$ , 910 ppm O<sub>3</sub> was compressed according to a RCM volume curve. The compression temperature  $T_C$  was determined in two ways: Directly from the simulation results and also by converting the pressure curve from the simulation into temperature, using the adiabatic core assumption. The latter method corresponds to the procedure used in experiments. It was found that the difference between the two temperatures is in the range of 30–40 K, amounting to less than 4% of the nominal value of  $T_C$ , which ranges from 1000 K to 1300 K. Detailed results on this can be found in the supplemental material (Fig. S5). More details about the experiment are given in Table 1 and in [15,16].

O<sub>3</sub> is produced using an ozone generator (Ozone Solutions TG-40 [17]). The amount of O<sub>3</sub> is measured using UV–VIS spectroscopy. For this purpose, a specific light signal with the wave length  $\lambda_1 = 254$  nm and  $\lambda_2 = 270$  nm was generated by a Deuterium–Halogen lamp (Ocean Optics DH-2000-BAL,[18]). This light signal passed through an optically accessible gas sample tube containing the O<sub>2</sub>/O<sub>3</sub> mixture delivered by the ozone generator via an optical fiber, before entering a spectrometer (Ocean Insight Flame UV–VIS Spectrometer [19]). The light signal gets attenuated by absorption of O<sub>3</sub> in the sample tube, allowing to measure the mole fraction of O<sub>3</sub> in the tube from the Lambert–Beer law (with the known standard-state absorption cross section of O<sub>3</sub> at 254 nm [20]), and the length of the test tube (54 mm).

The investigated gas mixtures are summarized in Table 2.

The mixtures were created using the partial pressure method. In all experiments, for a certain amount of added O<sub>3</sub>, the amount of O<sub>2</sub> was reduced accordingly to maintain an effective equivalence ratio of  $\phi = 2$ . Since NG ignites faster than CH<sub>4</sub>, less O<sub>3</sub> is added to the NG mixture. For the preparation of the desired fuel/air mixtures in cases where no ozone is added, air and fuel are first premixed in an external mixing chamber, before being filled to the RCM cylinder in the desired amount.

Undesired decomposition reactions of ozone during the long residence time in the mixing chamber was a concern, so in cases where O<sub>3</sub> was added, only fuel and argon were premixed in the mixing chamber, and this mixture was filled into the RCM cylinder separately

from  $O_2/O_3$ , immediately before an RCM experiment took place. This procedure is intended to prevent the  $O_3$  decomposition in the mixing vessel and keep the  $O_3$  content constant over a series of measurements. To ensure complete mixing, the residence time of the Ar/fuel/ $O_2/O_3$  mixture in the combustion chamber before compression was varied from about 1 to 5 min. This caused no change of ignition delay time or compression pressure, indicating that the fuel/ $O_2/O_3$ /Ar mixture had been fully mixed to a homogeneous state after one minute.

Also, to study whether any pre-reactions in the RCM cylinder would occur before compression, the  $O_3$  amount in the RCM after gas fill-in was measured at several times over a period of 5 minutes. It was found that the amount of  $O_3$  in the chamber did not change over 5 min. A similar procedure to guard against unintended ozone decomposition has been reported in the literature [21].

## 2.2. Simulation

Simulations with detailed chemistry were carried out using the in-house code HOMREA [22]. For simulations of the RCM process, a zero-dimensional adiabatic single-zone model was used. Simulation inputs were initial values of pressure, temperature, and gas mixture composition, as well as the prescribed volume curve. The volume curve was calculated from measured RCM pressure traces (inert gas mixtures), using an isentropic pressure–volume relation [23]. Inert gas mixtures with similar thermodynamic properties (in particular, with similar heat capacities) like their reacting analogues were obtained by replacing the oxygen ( $O_2$ ) in the reactants with nitrogen ( $N_2$ ). For sensitivity analyses, constant volume reactor simulations were used. For four-stroke engine cycles, the volume curve of a homogeneous reactor was prescribed as a function of crank angle, according to  $V(\varphi)$  from a crank-slider mechanism:

$$V(\varphi) = V_c + A \cdot \frac{s}{2} \cdot \left[ 1 - \cos \varphi + \frac{1}{L} \cdot \left( 1 - \sqrt{1 - L^2 \cdot (\sin \varphi)^2} \right) \right], \quad (1)$$

where  $V_c$  is the clearance volume,  $A$  is the cylinder cross section (calculated with the bore),  $s$  is the stroke, and  $L$  is the ratio of stroke and conrod length.

## 3. Mechanism development and analysis

A kinetic model is first obtained by combining PolyMech 2.0 [8], which includes 132 species and 749 reactions, and part of the ozone mechanism from [14]. The resulting mechanism will be referred to as PolyMech 2.01 in the following. The entire mechanism involves 761 elementary reactions among 133 species. Reactions between  $O_3$  and two minor components of NG,  $C_2H_6$  and  $C_3H_8$ , are not considered due to the low reactivity compared with  $O_3$  decomposition [24], as well as to keep the mechanism compact.

Fig. 1 compares IDTs simulated using PolyMech 2.01 with RCM measurements, of the mixtures listed in Table 2. The experiments with and without  $O_3$  addition were carried out at similar initial pressures and compression ratios. For experiments with  $O_3$  addition, initial temperatures were set to lower values to reduce reactivity.

The experimental results show that the addition of  $O_3$  reduces the IDTs for both  $CH_4$  and NG. PolyMech 2.01 predicts the IDTs for mixtures without ozone accurately. For mixtures with  $O_3$ , however, the predicted IDTs are significantly longer than measured values.

In RCM experiments with  $O_3$ -containing mixtures, the pressure at TDC  $P_C$  was slightly higher than for mixtures without  $O_3$ . This indicates that for  $O_3$ -containing mixtures, chemical reactions commenced already during the compression phase in mixtures with  $O_3$  addition. To investigate this phenomenon further, simulations of the RCM process for  $CH_4$  and  $CH_4 + O_3$  mixtures were performed. For each mixture, simulations with and without chemical reaction were compared to

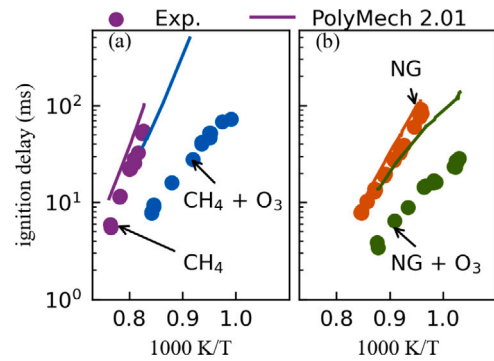


Fig. 1. Ignition delay times of (a)  $CH_4$  with and without  $O_3$  addition (b) natural gas with and without  $O_3$  addition, from experiments (Exp., symbols) and from simulations with PolyMech 2.01 (lines).

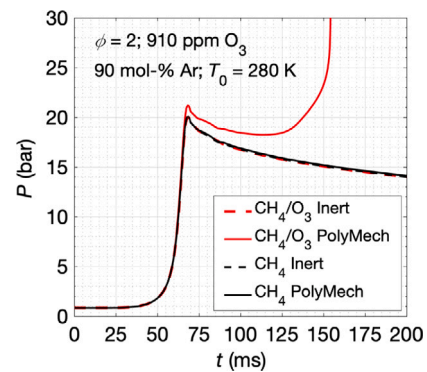


Fig. 2. Pressure profiles for a  $CH_4$  (black lines) and a  $CH_4/O_3$  mixture (red lines) from reactive (solid lines) and inert (dashed lines) simulations of an RCM compression. Pressures for the inert cases and reactive  $CH_4$  nearly overlap. Pressure trace for the  $CH_4/O_3$  mixture shows slightly increased pressure. (For interpretation of the references to color in this figure legend, the reader is referred to the web version of this article.)

assess the influence of reaction on temperature and pressure during the compression. The results are presented in Fig. 2.

For  $CH_4$  without ozone,  $P_C$  from reactive and inert simulations are nearly identical. This indicates that for this mixture, chemical reactions before TDC are insignificant.

For  $CH_4$  with ozone, however,  $P_C$  in the reacting simulation is by about 2 bar higher than the inert simulation, proving that reactions start before TDC. This observation is consistent with the results of Liao et al. [25], which report a similarly increased compression pressure for cases with  $O_3$  addition. As will be discussed later, the reactions responsible for the increased pressure are  $O_3$  decomposition and subsequent exothermal reactions.

To summarize, PolyMech 2.01 predicts reactivity of methane and natural gas without  $O_3$  addition well, but does not predict well when  $O_3$  is added. Our first hypothesis to explain the poor prediction was that some reaction rates in the ozone sub-mechanism were too slow. However, reactions in the ozone sub-mechanism have been well studied, [14,24], and their kinetic parameters are considered reliable. We also investigated the sensitivities of the IDTs with respect to these rate coefficients, and found that they are only weakly sensitive. We therefore reject the hypothesis of inaccurate reaction data in the ozone sub-mechanism as an explanation for the poor prediction seen in Fig. 1. Another explanation could be that some reactions in PolyMech 2.0 which exhibit only weak influence on ignition delay times of methane/air mixtures (and whose rate coefficients therefore likely have so far not been determined accurately) become more important for ignition when  $O_3$  is added. Uncertainties in the rate coefficients of these sensitive reactions have a greater influence on the IDTs for ozone-added mixtures.

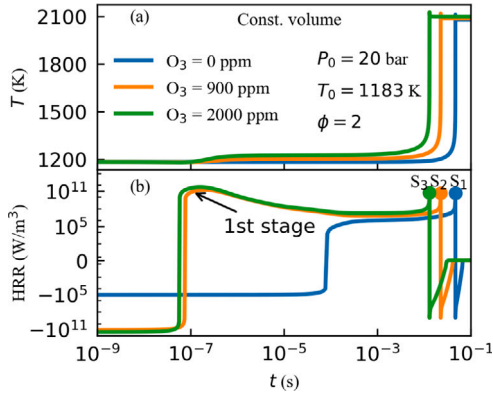


Fig. 3. Profiles of (a) temperature and (b) HRR with three different  $O_3$  concentrations for  $CH_4/O_3/O_2/Ar$  mixtures with PolyMech 2.01.

In order to identify these reactions, we perform sensitivity analyses. The initial conditions for  $\phi = 2$  mixtures are set to  $P_0 = 20$  bar and  $T_0 = 1183$  K, a representative condition at the TDC of RCM. A constant-volume homogeneous reactor model was chosen for the sensitivity studies.

The results of these simulations highlight that, in mixtures with  $O_3$ -addition, different stages occur in the reaction. As an example, profiles of temperature and heat release rate (HRR) with different  $O_3$  concentrations are shown in Fig. 3. Time is plotted in a log-scale to highlight the different stages of heat release. With  $O_3$  addition, there is a distinct first stage of heat release (near  $10^{-7}$  s). The peak HRR rate in this stage is comparable to the main HRR-stage (which appears close to  $10^{-1}$  s), but lasts much shorter, and therefore causes only a moderate temperature rise. This first temperature rise will be discussed in more detail below using the updated mechanism.

The main temperature rise occurs during the second stage of HRR. We define the ignition point as the time corresponding to the maximum HRR of the second-stage temperature rise, specifically points  $S_1$ ,  $S_2$  and  $S_3$  in Fig. 3.

One approach for sensitivity analysis is to perturb the rate coefficients  $k$  and evaluate the resulting change in IDTs (brute-force sensitivity). That is, one determines the quantity

$$S_{\tau,j} = \frac{k_j}{\tau_{\text{ign}}} \frac{\partial \tau_{\text{ign}}}{\partial k_j},$$

where  $k_j$  is the rate coefficient of reaction  $j$ , and  $\tau_{\text{ign}}$  is the IDT. Another approach is based on the sensitivity of composition at the ignition point with respect to the kinetic parameters  $k_j$ . For instance, the sensitivity of temperature at the ignition point,  $T_{\text{ign}}$ , with respect to  $k_j$ , is defined as

$$S_j = -\frac{k_j}{T_{\text{ign}}} \frac{\partial T_{\text{ign}}}{\partial k_j}. \quad (2)$$

Studies have shown that  $S_{\tau,j}$  and  $S_j$  have good alignment due to the existence of attracting manifolds [26,27]. The calculation of  $S_{\tau,j}$  requires multiple integrations of the ignition process. Also, numerical errors could arise from determining derivatives of IDTs with respect to velocity coefficients from simulating data. Therefore,  $S_j$  is used for sensitivity analyses in this work.

Based on the definition of  $S_j$ , increasing the rate coefficients of reactions with negative sensitivities will reduce the ignition delay time, while increasing the rate coefficients of reactions with positive sensitivities prolongs the ignition delay time. To compare the relative magnitude of sensitivities at different conditions, the sensitivity defined in Eq. (2) is normalized according to  $S_j = S_j / \|S\|$ , where  $\|S\|$  is the Euclidean norm of the vector formed by the  $S_j$ , similar as in [27].

Table 3  
Sensitive reactions and their uncertainties.

No.	Reaction	$G_i$	Source
R1	$CH_3 + HO_2 = CH_3O + OH$	2.0	[30]
R2	$H + HO_2 = H_2 + O_2$	2.00	[30]
R3	$C_2H_4 + OH = C_2H_3 + H_2O$	2.0	Estimated
R4	$CH_4 + O = CH_3 + OH$	2.51	[30]
R5	$C_2H_4 + CH_3 = C_2H_3 + CH_4$	3.16	[30]
R6	$CH_4 + H = CH_3 + H_2$	2.82	[30]
R7	$CH_4 + O_2 = CH_3 + HO_2$	3.98	[30]
R8	$C_2H_6 + HO_2 = C_2H_5 + H_2O_2$	2.66	[30]
R9	$C_2H_4 + H = C_2H_3 + H_2$	2.51	[30]
R10	$C_2H_6 + H = C_2H_5 + H_2$	2.24	[30]

A graphical rendition of the sensitivity analysis performed with PolyMech2.01 is given in the supplemental material (fig. S8). Its essential results for our study are: The two most significant reactions are  $H + O_2 = O + OH$  and  $CH_3 + HO_2 = CH_3O + OH$ . Reaction  $H + O_2 = O + OH$  is very important in the hydrogen sub-mechanism. With  $O_3$  addition, this reaction is becoming more sensitive due to the  $H_2$  production after the first stage ignition, as will be shown later.

Some of the reactions identified as being highly sensitive have thoroughly been studied and uncertainties are small. Reactions R1–R6 in Table 3, however, have relatively large uncertainties.

As a measure for the uncertainty of a rate coefficient, we define a parameter  $G$  [28] as

$$G = \frac{k^0}{k^{min}} = \frac{k^{max}}{k^0}, \quad (3)$$

where  $k^0$  is the nominal value of the rate coefficient, and  $k^{max}$  and  $k^{min}$  are the extreme upper and lower limits, respectively. With this definition, the distribution of rate coefficients on a log scale is centered around  $k^0$ , as  $\log(k^{min}) = \log(k^0) - \log(G)$  and  $\log(k^{max}) = \log(k^0) + \log(G)$ . Rate coefficients of the sensitive reactions are then modified within their uncertainty ranges to achieve an optimal fit between predicted and experimental IDTs.

The optimization target is to minimize the error

$$\varepsilon(k) = \sum_{j=0}^{n_p} |\tau_{\text{ign},j} - \tau_{\text{ign},j,\text{exp}}|,$$

where  $k$  is the vector of rate coefficients of dimension  $m$ , and  $n_p = 68$  is the number of RCM data points. The simulated and measured IDT for the  $j$ th RCM data point are  $\tau_{\text{ign},j}$  and  $\tau_{\text{ign},j,\text{exp}}$ , respectively. The genetic algorithm (GA) toolbox DEAP [29] is employed for this optimization; it was used with 50 individuals, crossover probability of 0.9 and mutation probability of 0.1.

Based on the updated mechanism with optimized rate coefficients for reactions R1–R6, the predicted IDTs for  $CH_4$  and  $CH_4 + O_3$  cases are close to the experimental data. However, there is still a significant deviation for NG, as shown in Fig. S1 (supplemental material). Therefore, another sensitivity analysis for  $CH_4$  and NG is performed as illustrated in Fig. S2. Reactions R7–R10 in Table 3 are also included as variables in the GA optimization, which can modify these variables within their uncertainties.

The optimized mechanism, PolyMech 3.0, is attached as a supplemental material along with its corresponding thermodynamic data file. Note that the optimized rate coefficients remain within their uncertainty ranges, and that the optimization never had to push the rate coefficients to their upper or lower limits. As shown in Fig. 4, PolyMech 3.0 predicts RCM IDTs reasonably well.

With PolyMech 3.0, it is now possible to explain the first stage temperature rise caused by  $O_3$  addition. With an  $O_3$  addition level of 900 ppm, there is a significant heat release around  $0.185 \mu\text{s}$  (HRR peak marked by point P in Fig. 5(a)). The dominant reactions at this point are presented in Fig. 5(b). Note that the decomposition  $O_3 \rightarrow O + O_2$  is endothermic. The exothermic reactions are mainly the recombination and oxidation of  $CH_3$ , as well as the H-abstraction of  $CH_4$  by OH. In

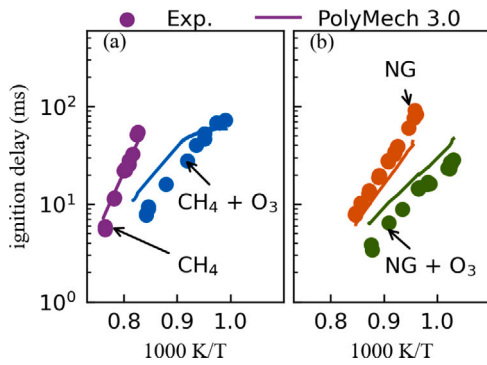


Fig. 4. Ignition delay times of (a) CH<sub>4</sub> with and without O<sub>3</sub> addition (b) natural gas with and without O<sub>3</sub> addition from experiments (symbols) and simulated with PolyMech 3.0 (curves).

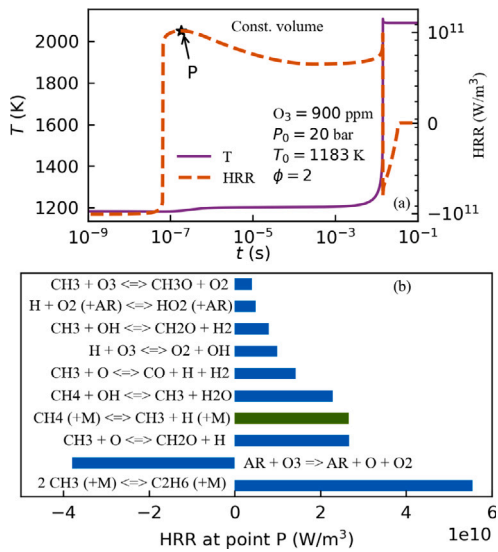


Fig. 5. (a) Temperature and HRR profiles of CH<sub>4</sub>/O<sub>3</sub>/O<sub>2</sub>/Ar mixtures with PolyMech 3.0, and (b) the dominant heat release reactions at the point P. Reactions with net forward and reverse progress are colored by blue and green, respectively. (For interpretation of the references to color in this figure legend, the reader is referred to the web version of this article.)

In this case, the first-stage temperature rise is about 20 K. It is plausible to expect that the initial temperature rise caused by this first stage process contributes to a shorter ignition delay time. To assess the importance of this effect, the IDTs for different initial temperatures are shown in Fig. 6, for mixtures with O<sub>3</sub> concentrations of 0 and 900 ppm. The circle and star markers,  $q_1$  and  $q_2$ , are the first two cases in Fig. 3. The diamond marker  $q_3$  represents an initial temperature and pressure of 1203 K and 20 bar, respectively, corresponding to the condition after the first stage ignition of  $q_2$ . It is seen that the ignition delay of  $q_3$  is still longer than  $q_2$ . Thus, the temperature rise alone is insufficient as an explanation for the earlier ignition with O<sub>3</sub> addition.

To more quantitatively assess the effects of O<sub>3</sub>-generated radicals and the effect of O<sub>3</sub>-decomposition induced temperature rise, Fig. 7 compares the temperature evolution for two simulation runs during auto-ignition in methane/oxygen/ozone mixtures in an isochoric-adiabatic system. The simulation for the red curve starts with unreacted mixture. Shortly after 10<sup>-7</sup> s, temperature rises slightly by the exothermal decomposition of O<sub>3</sub> (similar to Fig. 5). The main temperature rise is caused by ignition and oxidation of methane. The blue curve was obtained by taking the chemical composition from the “red” simulation and using this (with T<sub>0</sub> = 1183 K, p<sub>0</sub> = 20 bar) as the initial condition for a new simulation run. The ignition delay times for these two cases

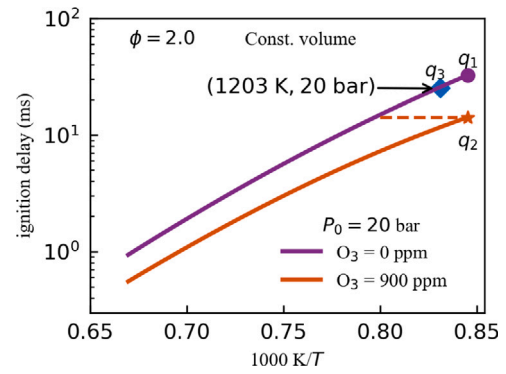


Fig. 6. Ignition delay times of CH<sub>4</sub>/O<sub>3</sub>/O<sub>2</sub>/Ar mixtures at different initial temperatures.

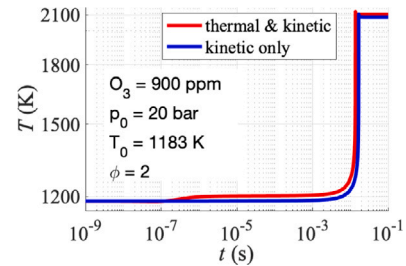


Fig. 7. Temperature profiles during isochoric auto-ignition in O<sub>2</sub>/CH<sub>4</sub>/O<sub>3</sub> mixtures with O<sub>3,0</sub> = 900 ppm, p<sub>0</sub> = 20 bar, T<sub>0</sub> = 1183 K. Red: Simulation includes both the kinetic and thermal effect of O<sub>3</sub> decomposition on IDT. Blue: Simulation includes the kinetic effect, but ignores the thermal effect of O<sub>3</sub> decomposition. Note the log-scale on the temperature axis. (For interpretation of the references to color in this figure legend, the reader is referred to the web version of this article.)

differ only by about 20%. We conclude that the initial temperature rise caused by the O<sub>3</sub>-decomposition here is only of minor influence for the subsequent auto-ignition of methane, which is more strongly affected by the kinetic effects induced by the O<sub>3</sub>-decomposition.

We also study how the change of chemical composition induced by the first stage ignition affects the subsequent auto-ignition. The reaction pathways at point P following the H and O atoms are shown in Fig. 8. The O radical produced from O<sub>3</sub> → O + O<sub>2</sub> is critical, as it subsequently produces OH and H radicals via reactions with CH<sub>4</sub> and CH<sub>3</sub>, and further promotes the H-abstraction of CH<sub>4</sub>. CH<sub>3</sub> undergoes several different reactions and forming C<sub>2</sub>H<sub>6</sub>, CH<sub>2</sub>O, H<sub>2</sub>, and CO. CH<sub>2</sub>O is relatively stable at this temperature range and do not react further. The profiles of species mole fractions in the constant volume simulation are shown in Fig. 9. Concentration of O radical initially increases due to O<sub>3</sub> decomposition and is fully consumed after the first stage ignition. Therefore, except for Ar, the most abundant species after the first stage ignition are O<sub>2</sub>, CH<sub>4</sub>, H<sub>2</sub>O, C<sub>2</sub>H<sub>6</sub>, CH<sub>2</sub>O, H<sub>2</sub>, and CO.

Combining Figs. 6–9, one can see that the ozone addition has two effects: the first stage temperature rise and the early production of reactive species such as H<sub>2</sub>. Both effects enhance reactivity and promote ignition, but the production of reactive species is the more pronounced effect.

#### 4. Parametric studies for four-stroke engine cycles

In this section, we use the improved mechanism to investigate the effect of ozone addition on the overall performance of polygeneration processes, specifically efficiencies of chemical energy storage and work output in four-stroke engine cycles.

The geometric compression ratio is set to 18 with an initial pressure of 0.6 bar. The bore, stroke and connecting rod are set to 0.0890, 0.0866, and 0.149 m, respectively. The displacement volume is 5.3875 ×

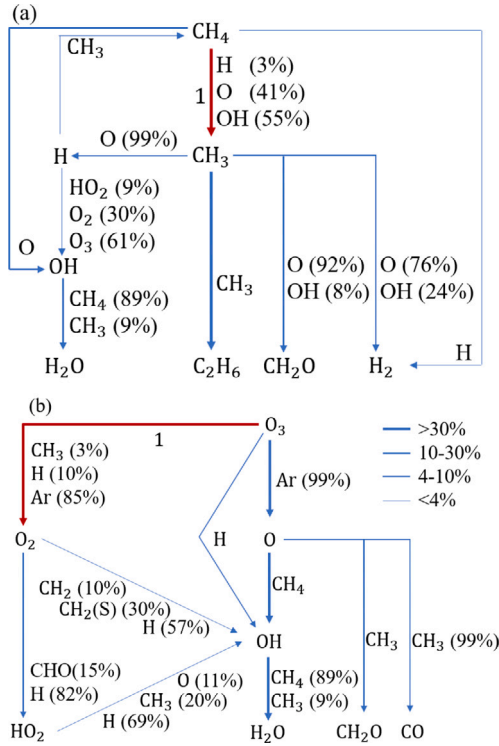


**Fig. 8.** The reaction pathway analyses following the atom (a) H and (b) O at the point P of Fig. 5. The highest molar flows ( $\text{kmol}/\text{m}^3 \text{ s}$ ) are represented by red arrows (marked with 1). The mole flows are normalized by the highest mole flow and represented by line thickness. (For interpretation of the references to color in this figure legend, the reader is referred to the web version of this article.)

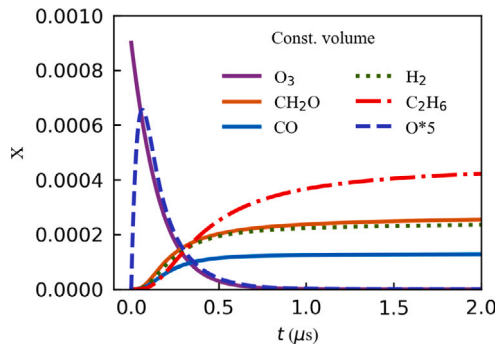


**Fig. 9.** The profiles of radical mole fractions in the first stage ignition for the case in Fig. 5.

$10^{-4} \text{ m}^3$ . The mixtures of  $\text{CH}_4/\text{O}_2/\text{O}_3/\text{Ar}$  at  $\phi = 2.0$  is of primary interest. The efficiencies are investigated by changing the engine speed,  $n$  in the unit of  $1/\text{min}$ ,  $\text{O}_3$  concentration and initial temperature.

Fig. 10 shows the temperature and  $\text{H}_2$  mole fraction profiles at two engine speeds,  $n = 1 \times 10^3$  and  $n = 1 \times 10^4$   $1/\text{min}$ , with  $\text{O}_3$  concentrations of 0 and 900 ppm. For the engine speed of  $n = 1 \times 10^3$   $1/\text{min}$ , with  $\text{O}_3$  addition, the ignition starts earlier and the peak temperature is slightly higher. However, at the end of the cycle, the species concentrations are comparable. When the engine speed is increased to  $n = 1 \times 10^4$   $1/\text{min}$ , the difference between with and without  $\text{O}_3$  addition becomes nontrivial. The mixture of  $\text{CH}_4/\text{O}_2/\text{Ar}$  does not ignite, and behaves like an inert compression/expansion cycle. While with  $\text{O}_3$  addition, the conversion starts and a certain amount of chemical energy is stored.

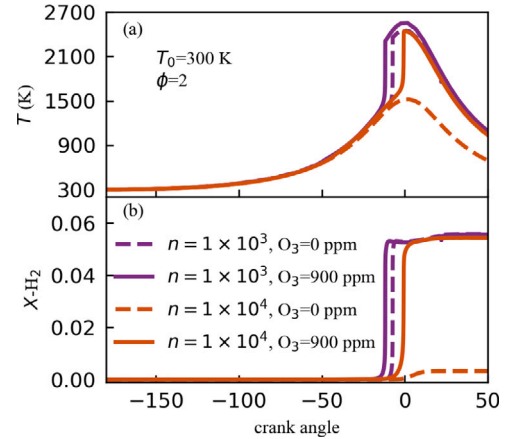


**Fig. 10.** Profiles of (a) temperature and (b)  $\text{H}_2$  mole fraction for  $\text{CH}_4/\text{O}_2/\text{O}_3/\text{Ar}$  mixtures with two different engine speeds and  $\text{O}_3$  concentrations.

The net work output is denoted as  $W$  and can be calculated by integrating the pressure over volume curve. The chemical energy stored in products other than  $\text{CH}_4$  is  $E_{\text{chem}} = \text{HHV}_p - \text{HHV}_{p,\text{CH}_4}$ , where HHV represents the higher heating value. We define the efficiencies of the chemical energy storage,  $\eta_E$ , and work output,  $\eta_W$ , as

$$\eta_E = \frac{E_{\text{chem}}}{\text{HHV}_R}, \eta_W = \frac{W}{\text{HHV}_R}, \text{ if } W > 0 \quad (4a)$$

$$\eta_E = \frac{E_{\text{chem}}}{\text{HHV}_R - W}, \eta_W = 0, \text{ if } W < 0 \quad (4b)$$

where subscript  $R$  represents reactants. Negative  $W$  represents work input, so the efficiency of work output is set to zero in this case. For  $\text{CH}_4/\text{O}_2/\text{O}_3/\text{Ar}$  mixtures of  $\phi = 2$  with  $\text{O}_3$  additions of 0 and 2000 ppm, the efficiencies at different initial temperatures and engine speeds are illustrated in Fig. 11. Without  $\text{O}_3$  addition, the efficiencies of chemical energy storage,  $\eta_E$ , approach zero at low initial temperatures and high engine speeds as shown in Figs. 11 (a). While it remains a reasonable value for almost the entire range investigated with 2000 ppm  $\text{O}_3$  addition. A similar trend is observed for the efficiencies of work output  $\eta_W$ . Therefore, the addition of  $\text{O}_3$  allows broader range of operating conditions including engine speeds and initial temperatures.

For practical applications, the engine speeds investigated could be higher than typical values. However, methane conversion can occur in a variety of reactors. Different engine speeds correspond to different residence times. If the reactor residence time is sufficiently long in comparison to the ignition timescale, the  $\text{O}_3$  addition has little effect on conversion efficiencies. While in scenarios requiring shorter residence times,  $\text{O}_3$  addition significantly promotes conversion. Furthermore, with ozone addition, the same conversion can be obtained with lower temperature.

## 5. Conclusions

A kinetic mechanism for the oxidation of methane/natural gas (NG) at fuel-rich conditions with doping of ozone is developed by a combination of numerical simulations and experiments in a rapid compression machine (RCM).

A simple combination of a methane/NG mechanism (PolyMech-2.01) with an ozone sub-mechanism significantly overpredicted the ignition delay times for  $\text{CH}_4 + \text{O}_3$  cases, even though the methane/NG mechanism predicts ignition well for pure methane fuels, and the reactions in the ozone mechanism all feature well-studied and accurate rate parameters. Sensitivity analyses identified reactions in the  $\text{CH}_4$  mechanism which are only of minor influence for ignition in hydrocarbon fuels, but become significantly more important when ozone is

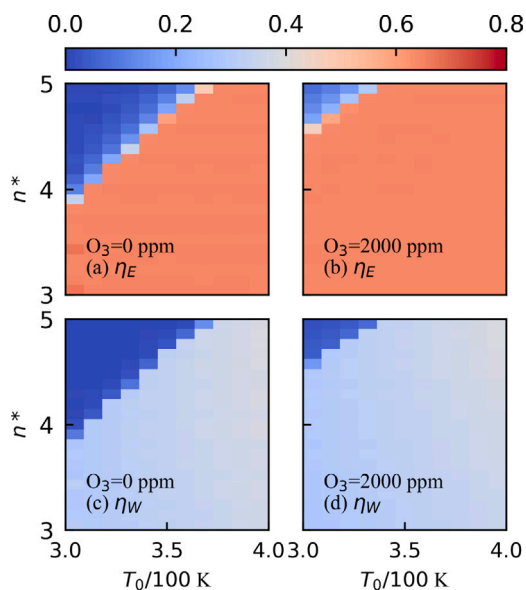


Fig. 11. The efficiencies of the chemical energy storage and net work output for  $\text{CH}_4/\text{O}_2/\text{O}_3/\text{Ar}$  mixtures of  $\phi = 2$  with  $\text{O}_3$  additions of 0 and 2000 ppm. (a) and (b):  $\eta_E$ ; (c) and (d):  $\eta_W$  at different initial temperatures and engine speeds, where  $n^* = \log_{10} \left( \frac{n}{1/\text{min}} \right)$ .

added. For some of these reactions, the rate parameters have relatively large uncertainties, and are therefore candidates for improvement of the combined methane/ $\text{O}_3$  mechanism. An optimization for the rate coefficients of these reactions was performed within their uncertainty ranges using a genetic algorithm. The optimized reaction mechanism, PolyMech 3.0, predicts the ignition delay times measured in a Rapid Compression Machine well. Qualitatively, the addition of ozone promotes ignition by inducing a first-stage temperature rise and producing reactive species, with the latter effect being more pronounced. The effect of ozone addition on the efficiencies of piston-engine based polygeneration processes was also studied by a parameter study. The results show that the addition of ozone enables a conversion at higher engine speeds and lower initial temperatures, and provides higher efficiencies under those conditions.

#### Declaration of competing interest

The authors declare that they have no known competing financial interests or personal relationships that could have appeared to influence the work reported in this paper.

#### Data availability

Data will be made available on request.

#### Acknowledgments

Financial support from the Deutsche Forschungsgemeinschaft (DFG, German Research Foundation) under projects no. 239920470 (MA1205/20-3) and 239927125 (SCHI 647/3-3) is gratefully acknowledged.

#### Appendix A. Supplementary data

Supplementary material is attached.

- Supplemental figures.

- Reaction Mechanism and Thermodynamic Data file for Poly-Mech3.0.
- Data files for measured RCM pressure traces.

Supplementary material related to this article can be found online at <https://doi.org/10.1016/j.jaecs.2023.100157>.

#### References

- [1] Dreizler A, Pitsch H, Scherer V, Schulz C, Janicka J. The role of combustion science and technology in low and zero impact energy transformation processes. *App Energy Combust Sci* 2021;7:100040.
- [2] Hegner R, Atakan B. A polygeneration process concept for HCCI-engines – modeling product gas purification and exergy losses. *Int J Hydrogen Energy* 2017;42(2):1287–97. <http://dx.doi.org/10.1016/j.ijhydene.2016.09.050>.
- [3] Atakan B, Kaiser SA, Herzler J, Porras S, Banke K, Deutschmann O, et al. Flexible energy conversion and storage via high-temperature gas-phase reactions: The piston engine as a polygeneration reactor. *Renew Sustain Energy Rev* 2020;133:110264.
- [4] Sen F, Kasper T, Bergmann U, Hegner R, Atakan B. Partial oxidation of methane at elevated pressures and effects of propene and ethane as additive: Experiment and simulation. *Z Phys Chem* 2015;229(6):955–76. <http://dx.doi.org/10.1515/zpch-2014-0576>.
- [5] Gossler H, Drost S, Porras S, Schießl R, Maas U, Deutschmann O. The internal combustion engine as a  $\text{CO}_2$ -reformer. *Combust Flame* 2019;207:186–95. <http://dx.doi.org/10.1016/j.combustflame.2019.05.031>.
- [6] Drost S, Xie W, Schiel R, Maas U.  $\text{CO}_2/\text{CH}_4$  Conversion to synthesis gas ( $\text{CO}/\text{H}_2$ ) in an internal combustion engine. *Proc Combust Inst* 2022;000:1–9. <http://dx.doi.org/10.1016/j.proci.2022.07.033>.
- [7] Atakan B. Gas turbines for polygeneration? A thermodynamic investigation of a fuel rich gas turbine cycle. *Int J Thermodyn* 2011;14(4):185–92.
- [8] Kaczmarek D, Herzler J, Porras S, Shaqiri S, Fikri M, Schulz C, et al. Plug-flow reactor and shock-tube study of the oxidation of very fuel-rich natural gas/DME/ $\text{O}_2$  mixtures. *Combust Flame* 2021;225:86–103.
- [9] Drost S, Schießl R, Maas U. Multi compression-expansion process for chemical energy conversion: Transformation of methane to unsaturated hydrocarbons and hydrogen. *Appl Energy Combust Sci* 2023;14:100129. <http://dx.doi.org/10.1016/j.jaecs.2023.100129>.
- [10] Daggett DL, Hendricks RC, Walther R, Corporan E. Alternate fuels for use in commercial aircraft. Boeing Company 2007;8(April).
- [11] Karacan CÖ, Ruiz FA, Coté M, Phipps S. Coal mine methane: A review of capture and utilization practices with benefits to mining safety and to greenhouse gas reduction. *Int J Coal Geol* 2011;86(2–3):121–56.
- [12] Porras S, Kaczmarek D, Herzler J, Drost S, Werler M, Kasper T, et al. An experimental and modeling study on the reactivity of extremely fuel-rich methane / dimethyl ether mixtures. *Combust Flame* 2020;212:107–22.
- [13] Schröder D, Banke K, Kaiser SA, Atakan B. The kinetics of methane ignition in fuel-rich HCCI engines: DME replacement by ozone. *Proc Combust Inst* 2021;38(4):5567–74.
- [14] Masurier JB, Foucher F, Dayma G, Dagaut P. Homogeneous charge compression ignition combustion of primary reference fuels influenced by ozone addition. *Energy Fuels* 2013;27(9):5495–505.
- [15] Drost S, Aznar MS, Schießl R, Ebert M, Chen JY, Maas U. Reduced reaction mechanism for natural gas combustion in novel power cycles. *Combust Flame* 2021;223:486–94.
- [16] Drost S, Werler M, Schießl R, Maas U. Ignition delay times of methane/diethyl ether (DME) blends measured in a rapid compression machine (RCM). *J Loss Prev Process Ind* 2021;71:104430. <http://dx.doi.org/10.1016/j.jlp.2021.104430>.
- [17] Ozone Solutions, Inc. TG series - Air cooled ozone generator, Model: TG-10, 20, 40, installation & operations manual. Tech. rep, Hull, IA, USA: Ozone Solutions, Inc.; 2019, p. 15, URL [https://ozonesolutions.com/content/TG-10-20-40\\_rev2a.pdf](https://ozonesolutions.com/content/TG-10-20-40_rev2a.pdf).
- [18] Ocean Optics, Inc. DH-2000 deuterium-halogen light source - Installation and operation manual. Tech. rep, Dunedin, FL, USA: Ocean Optics, Inc.; 2017, p. 27.
- [19] Ocean Insight, Inc. Flame - scientific-grade spectrometer - installation and operation manual. Tech. rep, Largo, FL, USA: Ocean Insight, Inc.; 2020, p. 21.
- [20] Gorshchev V, Serdyuchenko A, Weber M, Chehade W, Burrows J. High spectral resolution ozone absorption cross-sections – part 1: measurements, data analysis and comparison with previous measurements around 293 K. *Atmos Meas Tech* 2014;7(7):609–24.
- [21] Song Y, Foucher F. The impact of EGR components on ozone decomposition under engine relevant conditions in a rapid compression machine. *Fuel* 2020;276:118009.
- [22] Maas U, Warnatz J. Ignition processes in hydrogen-oxygen mixtures. *Combust Flame* 1988;74(1):53–69.
- [23] Goldsborough SS, Hochgreb S, Vanhove G, Wooldridge MS, Curran HJ, Sung CJ. Advances in rapid compression machine studies of low- and intermediate-temperature autoignition phenomena. *Prog Energy Combust Sci* 2017;63:1–78.

- [24] Sun W, Gao X, Wu B, Ombrello T. The effect of ozone addition on combustion: Kinetics and dynamics. *Prog Energy Combust Sci* 2019;73:1–25.
- [25] Liao W, Kang S, Chu Z, Liu Z, Wang Y, Yang B. Exploring the low-temperature oxidation chemistry with ozone addition in an RCM: A case study on ethanol. *Combust Flame* 2022;237:111727. <http://dx.doi.org/10.1016/j.combustflame.2021.111727>.
- [26] König K, Maas U. Sensitivity of intrinsic low-dimensional manifolds with respect to kinetic data. *Proc. Combust. Inst.* 2005;30(1):1317–23.
- [27] Ji W, Ren Z, Law CK. Evolution of sensitivity directions during autoignition. *Proc Combust Inst* 2019;37(1):807–15.
- [28] Tomlin AS, Agbro E, Nevrlý V, Dlabka J, Vašínek M. Evaluation of combustion mechanisms using global uncertainty and sensitivity analyses: A case study for low-temperature dimethyl ether oxidation. *Int. J. Chem. Kinet.* 2014;46(11):662–82.
- [29] Fortin F-A, Marc-André Gardner U, Parizeau M, Gagné C. DEAP: Evolutionary algorithms made easy. *J Mach Learn Res* 2012;13:2171–5.
- [30] Baulch DL, Bowman CT, Cobos CJ, Cox RA, Just T, Kerr JA, et al. Evaluated kinetic data for combustion modeling: Supplement II. *J. Phys. Chem. Ref. Data* 2005;34(3):757.